Journal of Membrane Science 593 (2020) 117427

Contents lists available at ScienceDirect

Journal of Membrane Science

journal homepage: www.elsevier.com/locate/memsci

Influence of temperature on gas transport properties of tetraaminodiphenylsulfone (TADPS) based polybenzimidazoles

Kevin A. Stevens[a,b,1], Joshua D. Moon[a,1], Hailun Borjigin[c], Ran Liu[c], Ronald M. Joseph[c], Judy S. Riffle[c], Benny D. Freeman[a,*]

[a] John J. McKetta Jr. Department of Chemical Engineering, The University of Texas at Austin, 2501 Speedway, Austin, TX, 78712, USA
[b] ExxonMobil Chemical Company, Baytown, TX, 77520, USA
[c] Department of Chemistry, Macromolecules Innovations Institute, Virginia Tech, Blacksburg, VA, 24061, USA

A B S T R A C T

Polybenzimidazoles have been the focus of increasing study due to their good H_2/CO_2 separation properties and high thermal stability. Gas transport properties of a series of polybenzimidazoles based on a tetraaminodiphenylsulfone (TADPS) monomer have been characterized at temperatures from 35 to 190 °C. Permeability increases with increasing temperature for all gases, and activation energies of permeation increase with increasing gas size with the exception of CO_2. CO_2 exhibits a lower activation energy of permeation than H_2 or He, presumably due to strong sorption effects. Gas separations with TADPS-based PBIs are strongly size selective, with CO_2/N_2, CO_2/CH_4, and N_2/CH_4 selectivities decreasing with increasing temperature. However, H_2/CO_2 selectivities increase with increasing temperature due to a lower activation energy of permeation for CO_2 than for H_2. All PBIs tested move toward the upper right on the H_2/CO_2 upper bound as temperature increases. Estimated diffusivities increase significantly with temperature, indicating high activation energies of diffusion that are consistent with the strongly size-sieving nature of these materials.

1. Introduction

Polybenzimidazoles (PBIs) are a class of highly thermally stable aromatic polymers [1]. PBIs have recently been studied for use as gas separation membranes because of their attractive H_2/CO_2 separation capabilities at high temperatures [2–9]. Membranes with high thermal stability could offer an economical and energy efficient alternative to conventional technologies for high temperature carbon capture operations (e.g., 150 °C or more), such as separating effluent streams from water-gas shift reactors [10–12]. However, few existing membrane materials can withstand such aggressive environments, necessitating study of more advanced materials such as PBIs.

The most common PBI studied in the literature is *m*-PBI, known commercially as Celazole® [4,6,13,14]. *m*-PBI has high thermal stability, with a degradation temperature above 600 °C, and a very rigid molecular structure with a T_g of approximately 416 °C [13]. Permeation experiments with *m*-PBI hollow fibers have been conducted at temperatures ranging from 250 to 350 °C and show permeances as high as 500 GPU (1 GPU = 10^{-6} cm^3 (STP)/(cm^2 s cmHg)) with H_2/CO_2 selectivities exceeding 15 [4,6]. One challenge of working with *m*-PBI, however, is its limited solubility in common organic solvents [14]. Developing new PBI materials with attractive transport properties that are more soluble in common solvents could potentially simplify the hollow fiber spinning process and catalyze design of better materials for such separations.

Several studies have examined the effect of chemical structure on transport properties of PBIs. *m*-PBI is typically synthesized from 3,3′-diaminobenzidine (DAB) and isophthalic acid (IPA) [1]. Kumbharkar et al. incorporated alternative diacid chemistries, including 5-*tert*-butyl isophthalic acid (BuI) and 4,4'-(hexafluoroisopropylidene)bis(benzoic acid) (HFA) [13]. The use of BuI and HFA resulted in 18- and 20-fold increases, respectively, in permeability for several gases, including H_2, at 35 °C relative to *m*-PBI by increasing free volume [13]. Kumbharkar also studied the effect of *N*-substitution (i.e., substitution of the imidazole hydrogen) on PBI transport properties at 35 °C [7,15]. *N*-substitution resulted in up to a 38-fold increase in H_2 permeability in a 4-*tert*-butylbenzyl-substituted PBI relative to *m*-PBI, and larger gases exhibited more substantial permeability increases (e.g., a 128-fold increase for CH_4) than smaller gases [7] through manipulation of free volume.

Li et al. studied the effect of varying diacid chemistry on high-temperature H_2/CO_2 separations for several fluorinated diacids as well as a diacid containing a phenylindane moiety [3]. Inclusion of the fluorinated and phenylindane groups yielded significantly increased

* Corresponding author.
E-mail address: freeman@che.utexas.edu (B.D. Freeman).
[1] Both authors contributed equally to this manuscript.

https://doi.org/10.1016/j.memsci.2019.117427
Received 25 April 2019; Received in revised form 21 June 2019; Accepted 27 August 2019
Available online 29 August 2019
0376-7388/

Table 1
Polybenzimidazole structures considered.

Name	Structure	T_g (°C)	Ref.
TADPS-TPA	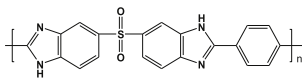	480	[17]
TADPS-IPA	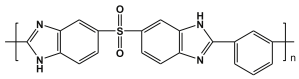	447	[17]
TADPS-OBA	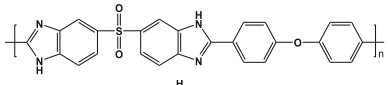	428	[17]
m-PBI	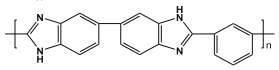	416	[13]

permeabilities at high temperatures. Hydrogen permeabilities at 250 °C increased to 997 Barrer for a hexafluoroisopropylidene-containing structure, compared to 77 Barrer for *m*-PBI [3]. Activation energies of permeation also decreased as a result of changing the backbone structure and disrupting chain packing, and the structures with the highest permeabilities had the lowest activation energies of permeation [3]. Finally, Han et al. studied the temperature dependence of a PBI made via a thermal rearrangement process (TR-PBI) [16]. The thermal rearrangement process resulted in very high permeabilities (e.g., H_2 permeability of 1779 Barrer with a H_2/CO_2 selectivity of 1.1 at 25 °C) and low activation energies of permeation (e.g., −1.48 and −4.93 kJ/mol for H_2 and CO_2, respectively) [16].

We recently reported the synthesis of a new series of TADPS-based PBIs [17], the structures of which are shown in Table 1. TADPS-based polybenzimidazoles have higher glass transition temperatures than *m*-PBI due to the addition of the sulfonyl moiety, and the films were thermally stable to above 400 °C [17]. Additionally, polymer solubility in common organic solvents was improved relative to *m*-PBI [17]. The initially reported permeabilities were limited to four gases at 35 °C without special sample drying protocols, but this work included care to ensure that all polymer samples were free of water. This study reports the temperature-dependence of permeability in TADPS-based PBIs alongside *m*-PBI to further elucidate structure/property relationships for PBI transport at elevated temperatures. Gas permeabilities increased with temperature for all samples tested. Furthermore, both H_2 permeability and H_2/CO_2 selectivity increased with increasing temperature for the TADPS-based PBIs. Analysis of estimated diffusivities revealed high activation energies of diffusion.

2. Background

The solution-diffusion model is given by Ref. [18]:

$$P = D \times S \tag{1}$$

where P, D, and S are the gas permeability, diffusivity, and solubility coefficients, respectively. Permeability is defined as [18]:

$$P = \frac{Nl}{\Delta p} \tag{2}$$

where N is the steady state flux of gas through the polymer, l is the membrane thickness, and Δp is the differential pressure across the membrane.

Permeability, diffusivity, and solubility typically follow Arrhenius-van't Hoff relationships with temperature [19]:

$$P = P_0 e^{\frac{-E_P}{RT}} \tag{3}$$

$$D = D_0 e^{\frac{-E_D}{RT}} \tag{4}$$

$$S = S_0 e^{\frac{-\Delta H_S}{RT}} \tag{5}$$

where P_0, D_0, and S_0 are exponential pre-factors, T is the experimental temperature, R is the gas constant, and E_P, E_D, and ΔH_S are the activation energies of permeation and diffusion and enthalpy of sorption, respectively. E_P, E_D, and ΔH_S are related by Ref. [19]:

$$E_P = E_D + \Delta H_S \tag{6}$$

Diffusion coefficients can be calculated by Equation (1) from permeability and solubility data. Alternatively, kinetic sorption or transient permeation data can be used to determine diffusion coefficients using the so-called "time lag" method [18]. For example, De Angelis et al. adapted the time lag method to calculate diffusivities directly from transient permeation data, where the diffusion coefficient is approximated based upon the time required to reach steady-state flux and the sample thickness [20].

Activation energies of diffusion often scale linearly with the square of penetrant diameter [18,21–23]:

$$E_D = m d_i^2 + y \tag{7}$$

where d_i is the gas diameter, and m and y are empirical parameters. The relationship between gas size and transport properties can be examined in the absence of diffusivity data using the activation energy of permeation (cf., Equation (6)). There are a variety of gas diameters that can be used for the analysis of gas diffusion in polymers [18,23,24]. Robeson regressed diffusion diameters based on a database of experimental diffusivities and upper bound correlations and found that these diffusion diameters were more representative for correlation of gas transport properties in polymers than prior zeolite-based kinetic diameters [23,24]. Transport properties of high free volume polymers such as thermally-rearranged (TR) polymers and polymers of intrinsic microporosity (PIMs) were found to correlate better with gas diffusion diameters than kinetic diameters [23]. Both gas diffusion and kinetic diameters will be employed in this study to better understand how transport properties of highly aromatic, low free volume polymers such as PBIs correlate with gas molecule size.

3. Experimental methods

3.1. Polymer synthesis and film preparation

Synthesis and film formation of TADPS-based PBIs have been described previously [17]. Films of *m*-PBI were cast using the following method. A dope solution of *m*-PBI (S26, 26% solids by weight in *N,N*-dimethylacetamide (DMAc)) was purchased from PBI Performance Products, Inc. (Charlotte, NC) and contained 1.5 wt% lithium chloride as a stabilizer. The solution was diluted to 2 wt% polymer with DMAc, filtered through a 0.45 μm PTFE filter into a clean scintillation vial, sonicated for 30 min, and cast onto a clean glass plate inside a glass ring. The film was held under full vacuum at room temperature overnight. The temperature was increased to 60 °C for 4 h and then 100 °C for 1 h. The film was delaminated from the glass plate using deionized water and boiled in water for 4 h to remove any residual DMAc. Lithium chloride in the film was extracted by soaking the boiled film in DI water for 24 h, changing the water multiple times. Lithium chloride removal was verified by ion chromatography. The final film was dried at 140 °C under full vacuum overnight. Complete solvent removal was verified by thermogravimetric analysis.

3.2. Gas permeability measurements

The permeabilities of H_2, He, N_2, CH_4, and CO_2 in four PBIs were measured over a range of temperatures by a constant-volume, variable-pressure method [25]. Downstream pressure was measured by an MKS Baratron 631C (MKS Instruments, Andover, MA) with a range of 0–10 Torr, and the upstream pressure was recorded with a Honeywell

STJE (Honeywell Sensotec, Columbus, OH) with a 150 psig (11.4 bara) range. Films of uniform thickness were mounted to brass support disks using Master Bond EP46HT-2 epoxy (Master Bond Inc., Hackensack, NJ) with a separate glass fiber filter backing to protect the polymer film. Epoxy was cured for 3 h at 140 °C followed by 3 h at 180 °C. Samples were loaded in a modified CF flange (i.e., knife-edge and copper gasket seal) over a porous stainless steel disk for mechanical support. The sample holder was attached to the permeation system, housed in a Thermo Fisher Scientific Heratherm OMH60 oven (Waltham, MA). The sample was degassed under vacuum at 190 °C overnight with a liquid nitrogen trap equipped. For fragile samples, the film was first allowed to degas at 35 °C for 24 h to minimize chances of film fracture caused by rapid contraction upon initial drying, then degassed overnight at 190 °C. The downstream pressure rise was measured at upstream pressures of 3–10 atm. Care was taken to prevent ambient atmosphere from entering the system after degassing to limit exposure of the samples to water, since PBIs are hygroscopic [17,26]. He, H_2, CH_4, N_2, and CO_2 permeabilities were measured in the order listed at decreasing temperatures of 190, 150, 125 (N_2 and CH_4 only), 100, 50 (He, H_2, and CO_2 only), and 35 °C (He, H_2, and CO_2 only). Pressure was limited to 10 atm to minimize any CO_2 conditioning. The largest gases, N_2 and CH_4, were not tested at temperatures below 100 °C due to low permeabilities, which were near the detection limit of the apparatus.

3.3. Density measurements

The densities of TADPS-TPA, TADPS-IPA, TADPS-OBA, and *m*-PBI were measured at ambient temperatures under dry conditions. Stainless steel containment vessels were constructed from a 1/2 inch Swagelok® cell, a valve, and a foot-long, 1/8 inch length of stainless steel tubing to give a long diffusional path length between the end of the tube and the valve seat. The samples were placed in the vessels, and the samples and vessels were heated to 190 °C for 24 h under full vacuum in a vacuum oven with the valve open to evacuate the cell. The oven was purged with air dried using a Drierite desiccant column while the oven was still above 100 °C. The oven was opened, and the valves were immediately closed to prevent moisture from entering the sample chamber.

The containment vessels were allowed to cool and were transferred into a dry glove box actively purged with UHP N_2. After a relative humidity of < 0.1% was reached as measured by a digital hygrometer (Fisher Scientific, Pittsburgh, PA), the samples were removed from the vessels, and density measurements were performed while below 0.1% relative humidity. The densities of three samples of each polymer were measured at room temperature several times with a density kit based on Archimedes' principle using *n*-heptane, selected for no solvent uptake and low surface tension during density measurements. Fractional free volumes were calculated using a group contribution method [21,27,28].

4. Results and discussion

4.1. Gas permeability measurements

Permeabilities of H_2, He, N_2, CH_4, and CO_2 were measured at several temperatures in three TADPS-based PBIs and *m*-PBI. Over the range of temperatures tested, the permeabilities of H_2 and He in TADPS-based PBIs and *m*-PBI were invariant with upstream pressure, within the uncertainty of the measurements. CO_2 exhibited some decrease in permeability with increasing pressure at lower temperatures, consistent with dual mode glassy polymer behavior [18], but other gases exhibited limited or no decrease with increasing pressure. The detailed permeability versus pressure data for each gas in each sample are presented in the Supplementary Information.

Permeabilities measured at 35 °C and 3 atm are presented in Table 2. The permeabilities at 35 °C of the TADPS-based PBIs were also reported previously [17], and these values for TADPS-TPA are included in Table 2 for reference. H_2 and He permeabilities are generally lower in this study than previously reported for TADPS-based PBIs, while CO_2 permeabilities in this study were higher, resulting in lower selectivities. The protocol for measuring permeabilities in this study included a degassing step at the initial temperature (i.e., 190 °C) prior to measurements, which would remove some residual water [1] and, consequently, impact the transport behavior of PBIs. Our previous study [17] did not include this high temperature drying step in the permeation system prior to beginning the permeability measurements, which likely leaves some residual water in the samples. Additionally, due to the change in drying protocol, the previous samples had a different thermal history than those in this study, and such differences in thermal history are known to influence permeation properties of glassy polymers [29]. The effects of residual water in these PBI membranes are being investigated further and will be reported in a future study.

The permeabilities of TADPS-IPA and TADPS-TPA exhibited *meta/para* relationships common to aromatic polymers [17,18,30]. *Meta*-linked isomers often exhibit lower permeabilities and higher selectivities than their *para*-linked analogs due to more restricted segmental mobility and enhanced packing efficiency [18]. As expected, TADPS-IPA, the *meta*-linked isomer, exhibited lower permeabilities (cf., Table 2) and higher selectivities than TADPS-TPA, the *para*-linked isomer, particularly at low temperatures. TADPS-OBA exhibited the highest permeabilities and lowest selectivities due to its ether oxygen moiety, which can increase polymer chain flexibility and lower T_g as observed in this study (cf., Table 1) [18].

Gas permeabilities at 190 °C and 3 atm are presented in Table 3. Li et al. and Berchtold et al. reported gas permeabilities at 250 °C and activation energies of permeation for *m*-PBI [3,5], which can be used to extrapolate permeabilities to 190 °C. These extrapolated values for several gases are included in Table 3. The permeabilities from these previous studies were different from those reported in this study, perhaps due to differences in thermal history, experimental methodology, or estimation techniques.

As shown in Table 3, for all samples and temperatures, permeability increased in the following order: $CH_4 < N_2 < CO_2 < H_2 < He$. In Fig. 1, permeabilities at 190 °C correlated with both gas diffusion diameter squared and gas kinetic diameter squared, as expected in strongly size-sieving materials [18,24]. A more linear relationship between log permeability and gas diameter squared is observed when kinetic diameters are used (R^2 of 0.97–0.98 for kinetic diameters and R^2 of 0.90–0.95 for diffusion diameters). Performing linear fits of log permeabilities vs. gas diameter squared yields slopes of −0.74 to −0.88 when kinetic diameters are used and slopes of −0.68 to −0.83 when diffusion diameters are used. Commonly used polymers such as polysulfone (PSF) [32] and Matrimid® [33] have slopes of −0.6 and −0.7, respectively, at 35 °C. The strong dependence of permeability on gas size in these polybenzimidazoles is indicative of strong size-sieving behavior at temperatures at least as high as 190 °C.

4.2. Effect of temperature on gas permeabilities

Permeabilities of CH_4, N_2, CO_2, H_2, and He in TADPS-TPA, TADPS-IPA, TADPS-OBA, and *m*-PBI at 3 atm from 35 to 190 °C (100–190 °C for CH_4 and N_2) are presented in Fig. 2. Permeabilities followed an Arrhenius relationship (i.e., Equation (3) where the log of permeability is linear with inverse temperature). CO_2 exhibited the weakest temperature dependence for each sample, while CH_4 displayed the strongest temperature dependence.

Activation energies of permeation were calculated by fitting the data in Fig. 2 to the Arrhenius relationship in Equation (3) and are presented in Table 4. All activation energies of permeation were positive, and the largest gases exhibited the highest activation energies of permeation, consistent with their strongly size-sieving behavior. Table 4 also presents E_P values for other polybenzimidazoles and a commercial polyimide, Matrimid®. Li et al. studied structurally-

Table 2
Permeabilities at 35 °C for TADPS-based PBIs and *m*-PBI.

Polymer	Permeabilities at 35 °C (Barrer) and 3 atm				
	He	H_2	N_2	CH_4	CO_2
TADPS-TPA, previously reported[a]	6.7 ± 0.2	5.5 ± 0.3	–	–	0.28 ± 0.02
TADPS-TPA	4.8 ± 0.5	3.7 ± 0.7	0.0054[d]	0.0017[d]	0.29 ± 0.03
TADPS-IPA	4.4[d]	3.2[d]	0.0031[d]	0.0013[d]	0.17[d]
TADPS-OBA	6.9 ± 0.2	5.4 ± 0.1	0.018[d]	0.0061[d]	0.87 ± 0.02
m-PBI	2.67 ± 0.07	2.4 ± 0.1	0.0025[d]	0.00052[d]	0.100 ± 0.003
m-PBI, previously reported[b]	1.05	0.6	0.0048[e]	0.0018[e]	0.16[e]
m-PBI, previously reported[c]	–	3.4[f]	0.0095[f]	–	0.22[f]

NOTE: Uncertainties calculated using propagation of errors [31].
[a] Data from Ref. [17].
[b] Data from Ref. [13].
[c] Data from Ref. [3].
[d] Extrapolated from higher temperature data using Equation (3).
[e] Estimated using solubility and an estimated diffusivity based on gas size.
[f] Estimated from activation energies of permeation and data at 250 °C.

modified polybenzimidazoles by varying the diacid monomer [3]. Their reference polymer, *m*-PBI, had similar activation energies of permeation to *m*-PBI measured in this study. Li et al. incorporated a 6F (i.e., hexafluoroisopropylidene) moiety into the polymer backbone [3], which typically disrupts chain packing and increases permeability [18]. The inclusion of 6F resulted in higher permeabilities and significantly lower activation energies of permeation due to their more open polymer structure [3]. Han et al. examined polybenzimidazoles created by a thermal rearrangement method [16]. This method typically results in an open polymer structure with high permeabilities, moderate selectivities, and low activation energies of permeation [34–38]. The resultant TR-PBI structure had very high permeability (1779 Barrer for H_2 at 25 °C) with low activation energies of permeation for small (i.e., H_2) or condensable (i.e., CO_2) gases [16]. Activation energies for TADPS-based PBIs were lower than those of *m*-PBI, indicating the sulfone group reduces some of their size-sieving ability. E_P values of all gases in TADPS-based PBIs were higher than those of 6F-PBI, TR-PBI, and Matrimid®.

The fractional free volume (FFV) of a polymer represents the amount of free space between polymer chains that is available for gas diffusion, and a polymer's FFV strongly impacts its gas permeabilities and activation energies of permeation [21,40]. Polymers with low FFV generally have lower permeabilities and higher diffusion selectivities than polymers with higher FFV due to enhanced size-sieving effects from their denser structures [18]. FFV can be estimated from measurements of polymer density and estimations of the occupied volume of molecular chains from group contribution methods [21,28]:

$$FFV = 1 - \frac{\rho(1.3\sum V_W)}{MW} \quad (8)$$

where ρ is the experimental polymer density, ΣV_w is the sum of van der Waals molar volumes of the polymer functional groups from group contribution theory, and *MW* is the molecular weight of the polymer repeat unit.

The FFVs and densities of the four PBIs investigated in this study are provided in Table 5 and compared with other PBIs and Matrimid®. *m*-PBI measured in this study had the lowest FFV of the polymers shown in Table 5, indicating it has the least FFV available for gas transport, which could provide the greatest barrier to gas diffusion. This low FFV value correlates with *m*-PBI having the highest activation energies of permeation of the compared polymers (cf., Table 4). 6F-PBI, TR-PBI, and Matrimid® all had much higher FFVs than the PBIs in this study, consistent with their higher permeabilities and lower activation energies of permeation relative to *m*-PBI and TADPS-based PBIs [3,16,39]. The difference between the FFVs of *m*-PBI measured in this study and the Li et al. study is likely due to differences in density measuring techniques and sample thermal treatment, as the densities used by Li et al. were measured by pyncometry on samples annealed at 250 °C rather than liquid displacement for samples annealed at 190 °C. Back calculation of the *m*-PBI van der Waals volume used in the calculations by Li et al. revealed slightly different values of van der Waals volumes from the ones employed in this study (cf., Table 5), which also contribute to differences in calculated FFV.

TADPS-IPA, the SO_2-containing analog of *m*-PBI, had slightly higher FFV than *m*-PBI (0.111 vs. 0.105), which resulted in its slightly higher permeabilities. The addition of the SO_2 moiety into the polymer backbone resulted in minimal to no decrease in the activation energy of permeation for most gases, possibly due to the retention of backbone stiffness provided by the SO_2 moiety. Two exceptions to this were the lower activation energies of permeation for CO_2 and CH_4 in TADPS-IPA, and two possible explanations are proposed for these differences. First, CH_4 and CO_2 are more soluble than gases like O_2 and N_2 and would be more strongly affected by changes in the enthalpies of sorption resulting from modifications of the backbone structure [18]. Additionally,

Table 3
Permeabilities at 190 °C for TADPS-based PBIs and *m*-PBI.

Polymer	Permeabilities at 190 °C (Barrer) and 3 atm					H_2/CO_2 ideal selectivity
	He	H_2	N_2	CH_4	CO_2	
TADPS-TPA	42 ± 4	31 ± 3	0.20 ± 0.02	0.12 ± 0.01	1.7 ± 0.2	18 ± 2
TADPS-IPA	42 ± 1	30.1 ± 0.8	0.170 ± 0.005	0.084 ± 0.002	1.22 ± 0.03	24.6 ± 0.9
TADPS-OBA	50 ± 1	38 ± 1	0.41 ± 0.01	0.307 ± 0.008	3.9 ± 0.1	9.7 ± 0.4
m-PBI	29.1 ± 0.8	22.1 ± 0.6	0.12 ± 0.01	0.10 ± 0.02	0.95 ± 0.03	23.3 ± 0.9
m-PBI (190 °C)[a] [3]	–	43.2[a]	0.345[a]	–	2.01[a]	21.5
m-PBI (190 °C)[a] [5]	–	33.4[a]	0.115[a]	0.075[a]	0.617[a]	

NOTE: Uncertainties calculated using propagation of errors [31].
[a] Estimated from activation energies of permeation and data at 250 °C. Values are provided for reference.

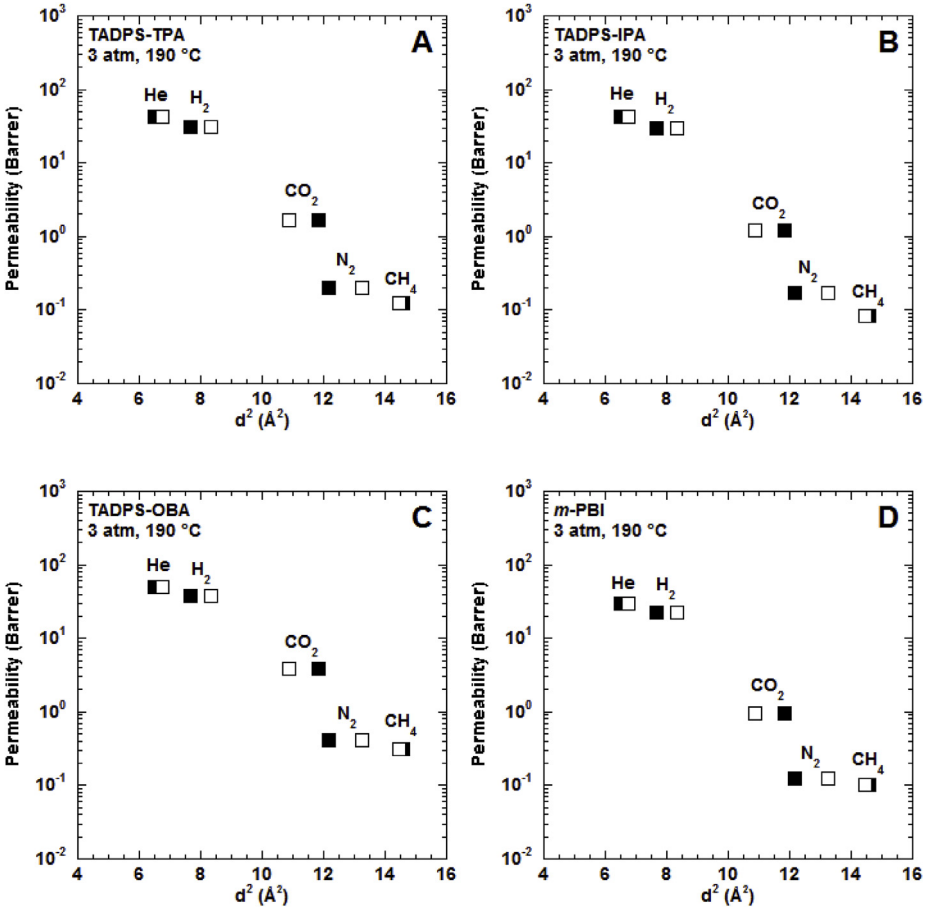

Fig. 1. Gas permeability at 190 °C and 3 atm as a function of gas diffusion or kinetic diameter squared [24] in: (A) TADPS-TPA, (B) TADPS-IPA, (C) TADPS-OBA, and (D) *m*-PBI. Gas diffusion diameters are shown in filled squares, and gas kinetic diameters are shown in unfilled squares.

larger molecules like CH_4 would have the least number of free volume elements available to them due to their large size, so any enlarging or creation of additional free volume elements due to changing polymer structure would have a more significant effect on CH_4 than on smaller gases. The addition of the SO_2 moiety may disrupt chain packing [17] and modify the size distribution of free volume elements, allowing CH_4 more access to free volume and lowering energy barriers for its diffusion and permeation. The additional free volume imparted by the SO_2 moiety slightly opens the polymer structure, thus increasing free volume.

TADPS-TPA had higher FFV than TADPS-IPA due to its more linear structure and more restricted chain packing, which is often observed for *para*-linked vs. *meta*-linked linear aromatic polymers [17,41–43]. This difference resulted in slightly higher permeabilities but little change in activation energies of permeation. While TADPS-TPA has a higher T_g than TADPS-IPA (480 °C vs. 447 °C), TADPS-TPA has a slightly lower sub-T_g β transition that may correlate with additional rotational mobility of its *para*-linked phenyl groups that could lead to increased gas permeabilities [17,26]. TADPS-OBA had the highest fractional free volume of the four PBIs in this study and correspondingly the highest permeabilities and lowest activation energies of permeation, due in part to its flexible ether linkage.

PBI permeabilities followed a general trend with 1/FFV observed in other families of polymers (i.e., the log of permeability is approximately linear with 1/FFV) [18,44,45]. Gas permeabilities vs. 1/FFV are presented in Fig. 3A. Larger gases such as N_2 and CH_4 are more strongly affected by differences in FFV. Gas permeabilities can be correlated with gas diameter squared divided by FFV to collapse the correlations from Figs. 1 and 3A onto a single curve [18,45,46]. Fig. 3B shows gas permeabilities plotted on a log scale vs. gas diffusion diameter squared divided by polymer FFV, and Fig. 3C shows a similar correlation using gas kinetic diameter squared. Gas permeabilities appear to correlate better with gas kinetic diameter than diffusion diameters, since all the data fall roughly on a single linear curve in Fig. 3C, whereas more variation is observed in Fig. 3B. Fig. 3D shows gas permeabilities vs. gas kinetic diameter squared divided by polymer FFV for all PBIs and gases across the entire temperature range studied (i.e., 35–190 °C). The slope of permeabilities plotted vs. kinetic diameter squared divided by FFV in Fig. 3D decreased at higher temperatures. Additional data, such as the temperature dependence of FFV, are needed to clarify the molecular origins of this behavior. FFV values would be expected to change with temperature based on polymer thermal expansion [47,48]. However, since polymer thermal expansion and density data at temperatures up to 190 °C are not easily accessible, this study approximated FFV values to be constant with temperature. Future study could elucidate the validity of this assumption.

Pure-gas selectivities for several gas pairs in TADPS-TPA at 3 atm were calculated and reported in Fig. 4 as a function of temperature. Similar trends were seen for the three other materials considered (cf., Figs. S5–S7). Selectivities for many, but not all, gas pairs decreased as temperature increased. N_2/CH_4 selectivity decreased from 2.2 at 100 °C to 1.6 at 190 °C. Selectivity of CO_2 over other gases (e.g., CO_2/CH_4 and CO_2/N_2) also decreased as temperature increased. In contrast, He/H_2 selectivity was approximately constant at values from 1.2 to 1.3 over the entire temperature range considered due to similar activation energies of permeation, as shown in Table 4.

Unlike that of most other gas pairs, H_2/CO_2 selectivity increased with increasing temperature. Since H_2 had a greater E_P than CO_2, as

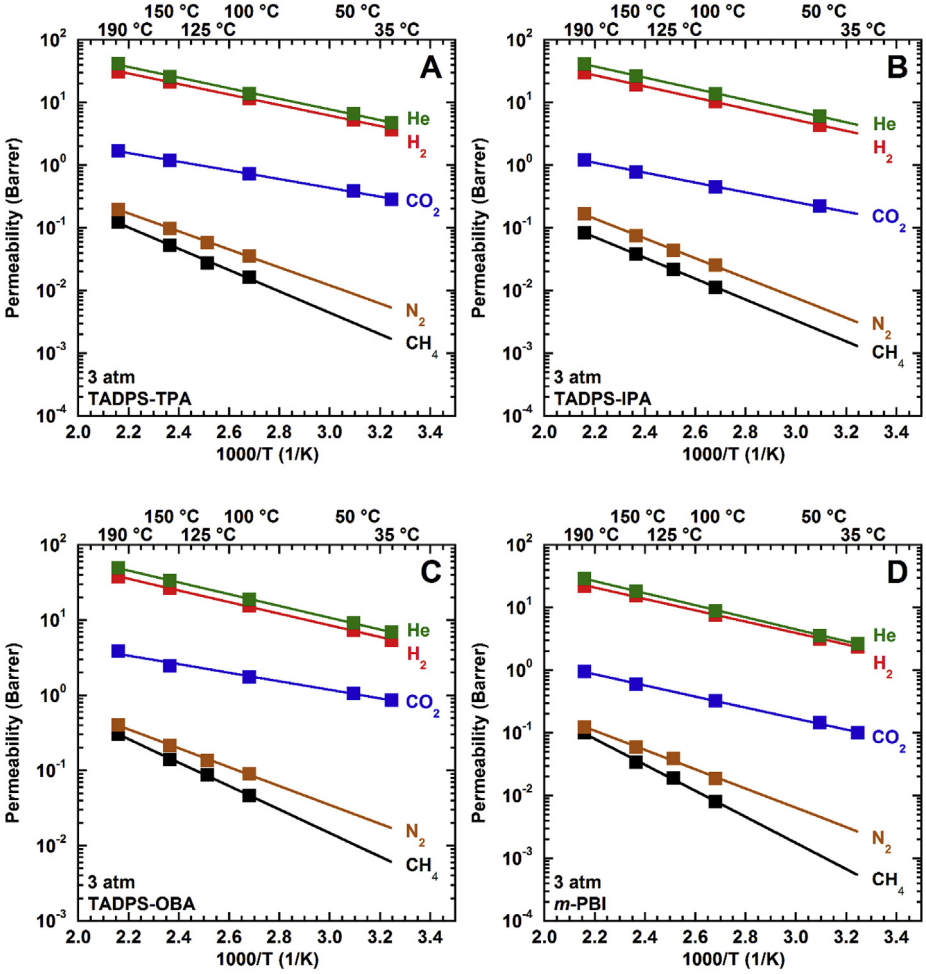

Fig. 2. The effect of temperature on gas permeability in: (A) TADPS-TPA, (B) TADPS-IPA, (C) TADPS-OBA, and (D) *m*-PBI. Solid lines represent fits to the Arrhenius model (Equation (3)). All data reported in this figure are at a feed pressure of 3 atm.

temperature increased, both H_2 and CO_2 permeabilities increased, but H_2 permeabilities increased to a greater extent, resulting in an increase in H_2/CO_2 selectivities with temperature. This can be more clearly seen in the Robeson upper bound in Fig. 5. As temperature increases from 35 °C (i.e., the leftmost data points for each sample) to 190 °C (i.e., the rightmost data points for each sample), H_2 permeability and H_2/CO_2 selectivity simultaneously increase. TADPS-OBA exhibited the greatest increase in selectivity over the temperature range considered, as it had the largest difference between E_P's for H_2 and CO_2, and *m*-PBI exhibited the least change in selectivity, due to similar E_P's for H_2 and CO_2.

Permeability/selectivity combinations for a range of other PBIs studied by Li et al. at 250 °C [3] are included in Fig. 5 for comparison. The samples considered here are in the lower permeability/higher selectivity range of PBIs, but extrapolations to 250 °C would yield combinations of permeability and selectivity in the region expected based on variations of chemical structure such as those reported by Li et al. [3] Upper bound plots for CO_2/CH_4, H_2/N_2, and He/H_2 gas pairs are included in Fig. S8 in the Supplementary Information section. CO_2/CH_4 permeabilities and selectivities move away from the upper bound as temperature increases, H_2/N_2 move approximately parallel to the upper

Table 4
Activation energies of permeation for TADPS-based PBIs, *m*-PBI, and other polymers.

	Activation energies of permeation (kJ/mol)				
	He	H_2	N_2	CH_4	CO_2
Gas Diffusion Diameter (Å)	2.55	2.77	3.49	3.817	3.44
Gas Kinetic Diameter (Å)	2.6	2.89	3.64	3.8	3.3
TADPS-TPA	16.2 ± 0.9	16 ± 1	28 ± 2	33 ± 2	13.3 ± 0.9
TADPS-IPA	17.1 ± 0.3	17.0 ± 0.3	30.5 ± 0.6	31.9 ± 0.8	14.9 ± 0.3
TADPS-OBA	15.0 ± 0.2	14.8 ± 0.2	23.9 ± 0.6	29.9 ± 0.5	10.8 ± 0.2
m-PBI	18.3 ± 0.3	17.4 ± 0.3	30.2 ± 0.9	40 ± 2	17.0 ± 0.3
m-PBI [3]	–	19.4	27.5	–	17.1
m-PBI [5]		18.5 ± 0.7	18.4 ± 10	23.4 ± 7.1	26.3 ± 2.0
6F-PBI [3]	–	8.36	11.02	–	0.391
TR-PBI [16]	–	−1.48	3.29	8.73	−4.93
Matrimid® [39]	13.6	–	20.7	26.3	9.8

Activation energies in kJ/mol. Gas diffusion and kinetic diameters from Robeson et al. [24]. Uncertainties from propagation of errors [31].

Table 5
Densities and FFV values of dried TADPS-based PBIs and *m*-PBI.

	Density (g/cm^3)	ΣV_w (cm^3/mol)[a]	FFV
TADPS-TPA	1.36 ± 0.01	184.7	0.121 ± 0.010
TADPS-IPA	1.38 ± 0.02	184.7	0.111 ± 0.017
TADPS-OBA	1.34 ± 0.01	233.5	0.125 ± 0.009
m-PBI	1.291 ± 0.004	164.4	0.105 ± 0.004
m-PBI [3]	1.31	154.8[b]	0.145
6F-PBI [3]	1.44	244.1[b]	0.145
TR-PBI [16]	1.262	231.2	0.267
Matrimid® [39]	1.238	294.0	0.144

[a] Sum of van der Waals molar volumes of polymer functional groups determined using group contribution theory [21,28].
[b] Back calculated from reported density and FFV values.

bound, and He/H_2 move horizontally to the right on the upper bound plot.

The unique behavior of simultaneously increasing H_2/CO_2 selectivity and gas permeabilities with increasing temperature is due to the size-sieving behavior of these polymers coupled with an E_P for CO_2 that is lower than might be expected based on its size. Gas diffusivities (and activation energies of diffusion) typically scale with gas molecule size [18,21,22], and activation energies of permeation are, therefore, expected to correlate with gas size for size-sieving polymers. As gas size increases, the energy required for a gas molecule to diffuse through a polymer increases, resulting in a higher activation energy for permeation. Fig. 6A shows E_P values plotted against gas diffusion diameter squared, and Fig. 6B shows E_P values plotted against gas kinetic diameter squared (cf., Equation (7)). Both gas diameters show similar trends. With the exception of CO_2, the activation energies of permeation for all gases for each PBI increased with increasing size, indicating strong size-sieving behavior [18,21,22].

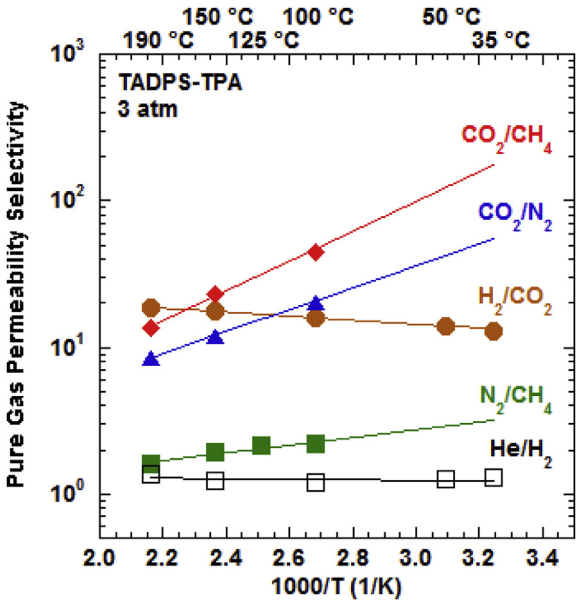

Fig. 4. Pure gas permeability selectivities for various gas pairs at 3 atm in TADPS-TPA as a function of temperature. Solid lines were calculated from Arrhenius fits of the data in Fig. 2.

CO_2 exhibited the lowest activation energy of permeation for each of the TADPS-based PBIs as well as *m*-PBI. CO_2 is the most condensable and soluble gas considered, and it would be anticipated to have the most exothermic (i.e., negative) enthalpy of sorption, which would

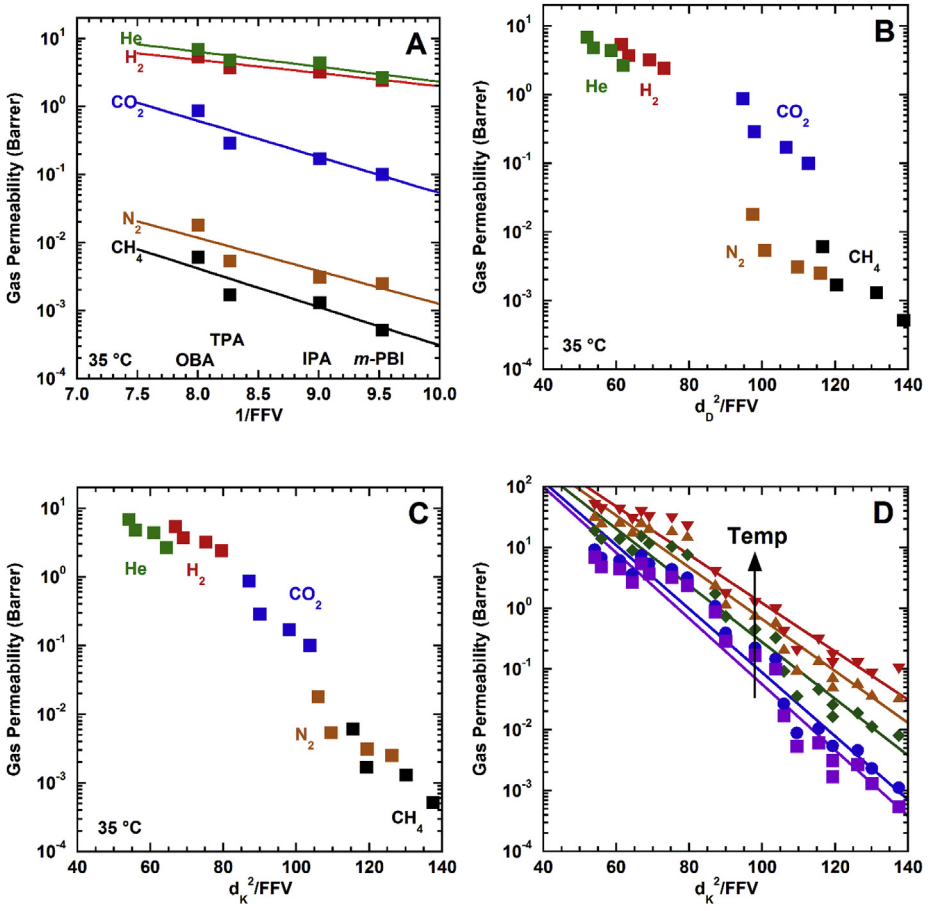

Figure 3. (A) Gas permeability at 3 atm and 35 °C as a function of inverse free volume. (B) Gas permeability vs. gas diffusion diameter squared divided by FFV at 35 °C and 3 atm. (C) Gas permeability vs. gas kinetic diameter squared divided by FFV at 35 °C and 3 atm. (D) Gas permeability vs. gas kinetic diameter squared divided by FFV at 3 atm across a range of temperatures (increasing upward: 35, 50, 100, 150, and 190 °C) for all gases tested. Solid lines represent a best fit using linear regression. Permeability values for N_2 and CH_4 for all polymers at 35 and 50 °C and permeability values for all gases for TADPS-IPA at 35 °C were extrapolated from higher temperature data using Equation (3).

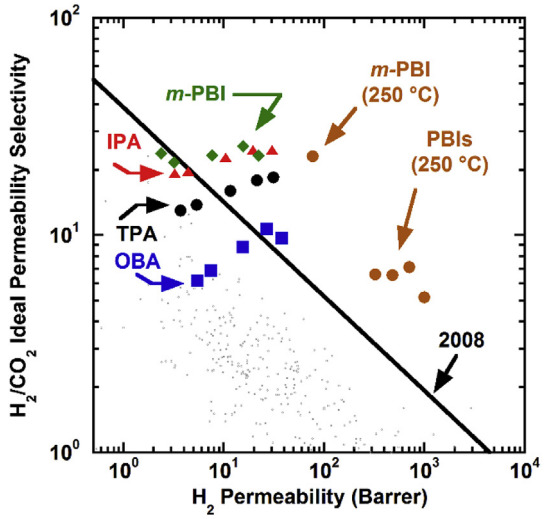

Fig. 5. H_2/CO_2 ideal selectivity plotted versus H_2 permeability for TADPS-IPA (red triangles), TADPS-TPA (black circles), TADPS-OBA (blue squares), and *m*-PBI (green diamonds) at temperatures increasing from left to right (i.e., 35, 50, 100, 150, 190 °C). Other PBIs measured at 250 °C are shown in dark orange circles [3]. The 35 °C data point for IPA is extrapolated using Equation (3). The line represents the 2008 upper bound [49], and the light gray data points are representative of many different polymers and are taken from the literature [49]. (For interpretation of the references to colour in this figure legend, the reader is referred to the Web version of this article.)

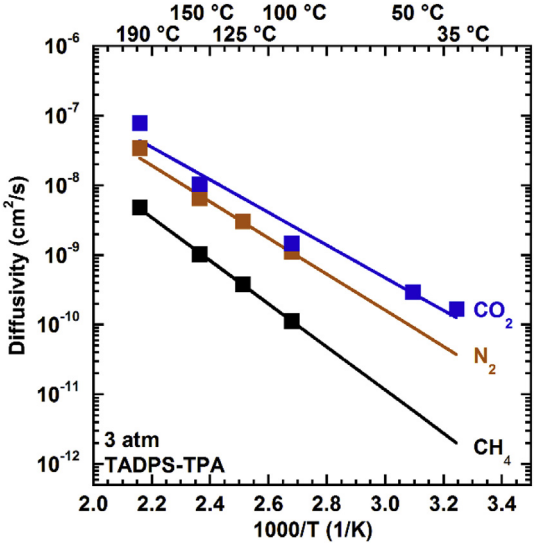

Fig. 7. Estimated diffusivity in TADPS-TPA at approximately 3 atm. Diffusivities were estimated using the time-lag method reported by De Angelis [20], and the solid lines represent Arrhenius fits.

result in a lower E_P. Additionally, favorable interactions between CO_2 and polar groups in these polymers may occur, further contributing to more exothermic sorption. The solubility behavior of CO_2 can be estimated through its permeability and diffusivity, discussed further below.

4.3. Temperature dependence of diffusivity

The temperature dependence of diffusion coefficients can provide more detail about the transport behavior of PBIs. The diffusion coefficients of faster gases (i.e., He and H_2) were too fast to be measured reliably. Diffusivities of CO_2, N_2, and CH_4 were estimated in TADPS-TPA using the time-lag method reported by De Angelis et al. [20] and are presented in Fig. 7 as a function of inverse temperature. Similar calculations can be performed for other PBIs, but variation in upstream pressure before steady state permeation was reached complicated the fitting procedure. TADPS-TPA provided the most complete data set and was considered here. As temperature increased, diffusion coefficients increased significantly. Gas size also plays a significant role in diffusivity. For example, CH_4, with a diffusion diameter of 3.817 Å, displayed an order of magnitude lower diffusivity at 100 °C than nitrogen, which has a diffusion diameter of 3.49 Å [24]. CO_2, the smallest gas considered for these estimations, exhibited the highest diffusivities. Diffusivities were too high to be reliably estimated for He and H_2.

Activation energies of diffusion can be calculated based on the data in Fig. 7 using Equation (4). These values are summarized in Table 6. As expected, larger gases show higher activation energies of diffusion (cf., Equation (7)). Larger methane molecules exhibited an activation energy of diffusion of 59 ± 4 kJ/mol, while smaller CO_2 molecules had an activation energy of diffusion of 45 ± 1 kJ/mol. Enthalpies of sorption, calculated as the difference between E_P and E_D according to Equation (6), correlate with penetrant condensability (i.e., critical temperature). Consistent with an earlier hypothesis, CO_2, the most condensable penetrant, exhibited the most exothermic enthalpy of sorption due to its high critical temperature [18] and potential to interact with polar groups [50] in these polymers. This effect resulted in its lower E_P values than other gases, including H_2, and the unique upper bound trends observed for H_2/CO_2. Solubility coefficients were calculated using the estimated diffusivities in Fig. 7 and are presented in the Supplemental Information (Fig. S9). CO_2, N_2, and CH_4 solubilities were estimated to decrease with temperature in TADPS-TPA. As expected, CO_2 exhibited the highest solubility. Future studies that measure temperature

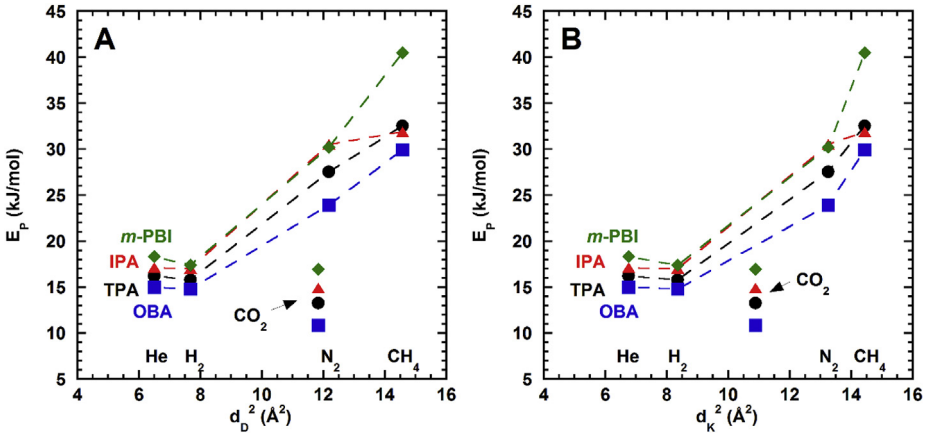

Fig. 6. Activation energy of permeation versus (A) gas diffusion diameter squared (d_D^2) and (B) gas kinetic diameter squared (d_K^2) (cf., Equation (7)). Dashed lines are guides for the eye.

Table 6
Activation energies of permeation, activation energies of diffusion, and enthalpies of sorption in TADPS-TPA at 3 atm.

Gas	Gas Diffusion Diameter [24]	Gas Kinetic Diameter [24]	Critical temperature (K) [18]	E_P	E_D	ΔH_S
CO_2	3.44	3.3	304.2	13 ± 1	45 ± 1	−32 ± 1
N_2	3.49	3.64	126.2	28 ± 2	50 ± 5	−22 ± 6
CH_4	3.817	3.8	190.6	33 ± 2	59 ± 4	−27 ± 4

Activation energies and enthalpies reported at 3 atm in kJ/mol.

dependence of gas sorption using direct experimental methods, such as pressure decay sorption, could further elucidate the roles of sorption and diffusion in these observed trends.

5. Conclusions

The temperature dependence of He, H_2, N_2, CH_4, and CO_2 permeabilities in TADPS-IPA, TADPS-TPA, TADPS-OBA, and *m*-PBI polybenzimidazoles was measured. Permeabilities increased with increasing temperature, and the activation energies of permeation increased with increasing gas size except for CO_2, which had the lowest activation energy of permeation for the TADPS-based PBIs. CO_2/N_2, CO_2/CH_4, and N_2/CH_4 selectivities decreased with increasing temperature, while H_2/CO_2 selectivities increased. All TADPS-based PBI samples moved towards the upper right on the H_2/CO_2 upper bound as temperature increased as a result of lower values of E_P for CO_2 than for H_2. Estimated diffusivities in TADPS-TPA increased significantly with temperature due to high activation energies of diffusion, consistent with the strongly size-sieving behavior of polybenzimidazoles.

Acknowledgements

The authors gratefully acknowledge financial support for the experimental work reported here from the Division of Chemical Sciences, Geosciences, and Biosciences, Office of Basic Energy Sciences of the U.S. Department of Energy through Grant DE-FG02-02ER15362. This material is based upon work supported in part by the National Science Foundation Graduate Research Fellowship Program under Grant DGE-1610403. Any opinions, findings and conclusions or recommendations expressed in this material are those of the authors and do not necessarily reflect the views of the National Science Foundation.

Appendix A. Supplementary data

Supplementary data to this article can be found online at https://doi.org/10.1016/j.memsci.2019.117427.

References

[1] T.-S. Chung, A critical review of polybenzimidazoles, J. Macromol. Sci., Part C 37 (1997) 277–301.
[2] J. Sánchez-Laínez, B. Zornoza, S. Friebe, J. Caro, S. Cao, A. Sabetghadam, B. Seoane, J. Gascon, F. Kapteijn, C. Le Guillouzer, G. Clet, M. Daturi, C. Téllez, J. Coronas, Influence of ZIF-8 particle size in the performance of polybenzimidazole mixed matrix membranes for pre-combustion CO_2 capture and its validation through interlaboratory test, J. Membr. Sci. 515 (2016) 45–53.
[3] X. Li, R.P. Singh, K.W. Dudeck, K.A. Berchtold, B.C. Benicewicz, Influence of polybenzimidazole main chain structure on H_2/CO_2 separation at elevated temperatures, J. Membr. Sci. 461 (2014) 59–68.
[4] R.P. Singh, G.J. Dahe, K.W. Dudeck, C.F. Welch, K.A. Berchtold, High temperature polybenzimidazole hollow fiber membranes for hydrogen separation and carbon dioxide capture from synthesis gas, Energy Procedia 63 (2014) 153–159.
[5] K.A. Berchtold, R.P. Singh, J.S. Young, K.W. Dudeck, Polybenzimidazole composite membranes for high temperature synthesis gas separations, J. Membr. Sci. 415–416 (2012) 265–270.
[6] S.C. Kumbharkar, Y. Liu, K. Li, High performance polybenzimidazole based asymmetric hollow fibre membranes for H_2/CO_2 separation, J. Membr. Sci. 375 (2011) 231–240.
[7] S.C. Kumbharkar, U.K. Kharul, Investigation of gas permeation properties of systematically modified polybenzimidazoles by N-substitution, J. Membr. Sci. 357 (2010) 134–142.
[8] K.C. O'Brien, G. Krishnan, K.A. Berchtold, S. Blum, R. Callahan, W. Johnson, D.L. Roberts, D. Steele, D. Byard, J. Figueroa, Towards a pilot-scale membrane system for pre-combustion CO_2 separation, Energy Procedia 1 (2009) 287–294.
[9] D.R. Pesiri, B. Jorgensen, R.C. Dye, Thermal optimization of polybenzimidazole meniscus membranes for the separation of hydrogen, methane, and carbon dioxide, J. Membr. Sci. 218 (2003) 11–18.
[10] T.C. Merkel, M. Zhou, R.W. Baker, Carbon dioxide capture with membranes at an IGCC power plant, J. Membr. Sci. 389 (2012) 441–450.
[11] S. Japip, K.-S. Liao, T.-S. Chung, Molecularly tuned free volume of vapor cross-linked 6FDA-durene/ZIF-71 MMMs for H_2/CO_2 separation at 150 °C, Adv. Mater. 29 (2017) 1603833.
[12] T. Yang, T.-S. Chung, High performance ZIF-8/PBI nano-composite membranes for high temperature hydrogen separation consisting of carbon monoxide and water vapor, Int. J. Hydrogen Energy 38 (2013) 229–239.
[13] S.C. Kumbharkar, P.B. Karadkar, U.K. Kharul, Enhancement of gas permeation properties of polybenzimidazoles by systematic structure architecture, J. Membr. Sci. 286 (2006) 161–169.
[14] W.S. Lyoo, J.H. Choi, S.S. Han, W.S. Yoon, M.S. Park, B.C. Ji, J. Cho, Preparation of organo-soluble poly[(2,2′-m-phenylene)-5,5′-bibenzimidazole] with high yield by homogeneous nitration reaction, J. Appl. Polym. Sci. 78 (2000) 438–445.
[15] S.C. Kumbharkar, U.K. Kharul, N-substitution of polybenzimidazoles: synthesis and evaluation of physical properties, Eur. Polym. J. 45 (2009) 3363–3371.
[16] S.H. Han, J.E. Lee, K.-J. Lee, H.B. Park, Y.M. Lee, Highly gas permeable and microporous polybenzimidazole membrane by thermal rearrangement, J. Membr. Sci. 357 (2010) 143–151.
[17] H. Borjigin, K.A. Stevens, R. Liu, J.D. Moon, A.T. Shaver, S. Swinnea, B.D. Freeman, J.S. Riffle, J.E. McGrath, Synthesis and characterization of polybenzimidazoles derived from tetraaminodiphenylsulfone for high temperature gas separation membranes, Polymer 71 (2015) 135–142.
[18] S. Matteucci, Y. Yampolskii, B.D. Freeman, I. Pinnau, Transport of gases and vapors in glassy and rubbery polymers, Materials Science of Membranes for Gas and Vapor Separation, John Wiley & Sons, Chichester, U.K., 2006, pp. 1–47.
[19] K. Ghosal, B.D. Freeman, Gas separation using polymer membranes: an overview, Polym. Adv. Technol. 5 (1994) 673–697.
[20] M.G. De Angelis, G.C. Sarti, A. Sanguineti, P. Maccone, Permeation, diffusion, and sorption of dimethyl ether in fluoroelastomers, J. Polym. Sci. B Polym. Phys. 42 (2004) 1987–2006.
[21] D.W.W. van Krevelen, Properties of Polymers, third ed., Elsevier, Amsterdam, 1997.
[22] P. Meares, The diffusion of gases through polyvinyl acetate, J. Am. Chem. Soc. 76 (1954) 3415–3422.
[23] L.M. Robeson, M.E. Dose, B.D. Freeman, D.R. Paul, Analysis of the transport properties of thermally rearranged (TR) polymers and polymers of intrinsic microporosity (PIM) relative to upper bound performance, J. Membr. Sci. 525 (2017) 18–24.
[24] L.M. Robeson, Z.P. Smith, B.D. Freeman, D.R. Paul, Contributions of diffusion and solubility selectivity to the upper bound analysis for glassy gas separation membranes, J. Membr. Sci. 453 (2014) 71–83.
[25] H. Czichos, T. Saito, L. Smith, Springer Handbook of Materials Measurement Methods, Springer Verlag, 2006.
[26] J.D. Moon, M. Galizia, H. Borjigin, R. Liu, J.S. Riffle, B.D. Freeman, D.R. Paul, Water vapor sorption, diffusion, and dilation in polybenzimidazoles, Macromolecules 51 (2018) 7197–7208.
[27] J.Y. Park, D.R. Paul, Correlation and prediction of gas permeability in glassy polymer membrane materials via a modified free volume based group contribution method, J. Membr. Sci. 125 (1997) 23–39.
[28] A. Bondi, van der Waals volumes and radii, J. Phys. Chem. 68 (1964) 441–451.
[29] A.H. Chan, D.R. Paul, Effect of sub-Tg annealing on gas transport in polycarbonate, J. Appl. Polym. Sci. 25 (1980) 971–974.
[30] Q. Liu, H. Borjigin, D.R. Paul, J.S. Riffle, J.E. McGrath, B.D. Freeman, Gas permeation properties of thermally rearranged (TR) isomers and their aromatic polyimide precursors, J. Membr. Sci. 518 (2016) 88–99.
[31] P.R. Bevington, D.K. Robinson, Data Reduction and Error Analysis for the Physical Sciences, McGraw Hill, Boston, 2003.
[32] J.S. McHattie, W.J. Koros, D.R. Paul, Gas transport properties of polysulphones: 1. Role of symmetry of methyl group placement on bisphenol rings, Polymer 32 (1991) 840–850.
[33] H. Zhao, Y. Cao, X. Ding, M. Zhou, Q. Yuan, Effects of cross-linkers with different molecular weights in cross-linked Matrimid 5218 and test temperature on gas transport properties, J. Membr. Sci. 323 (2008) 176–184.
[34] H.B. Park, C.H. Jung, Y.M. Lee, A.J. Hill, S.J. Pas, S.T. Mudie, E. Van Wagner, B.D. Freeman, D.J. Cookson, Polymers with cavities tuned for fast selective transport of small molecules and ions, Science 318 (2007) 254–258.
[35] D.F. Sanders, R. Guo, Z.P. Smith, K.A. Stevens, Q. Liu, J.E. McGrath, D.R. Paul, B.D. Freeman, Influence of polyimide precursor synthesis route and ortho-position functional group on thermally rearranged (TR) polymer properties: Pure gas

permeability and selectivity, J. Membr. Sci. 463 (2014) 73–81.
[36] D.F. Sanders, R. Guo, Z.P. Smith, Q. Liu, K.A. Stevens, J.E. McGrath, D.R. Paul, B.D. Freeman, Influence of polyimide precursor synthesis route and ortho-position functional group on thermally rearranged (TR) polymer properties: conversion and free volume, Polymer 55 (2014) 1636–1647.
[37] D.F. Sanders, Z.P. Smith, C.P. Ribeiro, R. Guo, J.E. McGrath, D.R. Paul, B.D. Freeman, Gas permeability, diffusivity, and free volume of thermally rearranged polymers based on 3,3′-dihydroxy-4,4′-diamino-biphenyl (HAB) and 2,2′-bis-(3,4-dicarboxyphenyl) hexafluoropropane dianhydride (6FDA), J. Membr. Sci. 409–410 (2012) 232–241.
[38] Z.P. Smith, D.F. Sanders, C.P. Ribeiro, R. Guo, B.D. Freeman, D.R. Paul, J.E. McGrath, S. Swinnea, Gas sorption and characterization of thermally rearranged polyimides based on 3,3′-dihydroxy-4,4′-diamino-biphenyl (HAB) and 2,2′-bis-(3,4-dicarboxyphenyl) hexafluoropropane dianhydride (6FDA), J. Membr. Sci. 415–416 (2012) 558–567.
[39] L. Ansaloni, M. Minelli, M.G. Baschetti, G.C. Sarti, Effect of relative humidity and temperature on gas transport in Matrimid®: experimental study and modeling, J. Membr. Sci. 471 (2014) 392–401.
[40] Y. Yampolskii, S. Shishatskii, A. Alentiev, K. Loza, Correlations with and prediction of activation energies of gas permeation and diffusion in glassy polymers, J. Membr. Sci. 148 (1998) 59–69.
[41] Y. Mi, S.A. Stern, S. Trohalaki, Dependence of the gas permeability of some polyimide isomers on their intrasegmental mobility, J. Membr. Sci. 77 (1993) 41–48.
[42] M.R. Coleman, W.J. Koros, Isomeric polyimides based on fluorinated dianhydrides and diamines for gas separation applications, J. Membr. Sci. 50 (1990) 285–297.
[43] H. Borjigin, Q. Liu, W. Zhang, K. Gaines, J.S. Riffle, D.R. Paul, B.D. Freeman, J.E. McGrath, Synthesis and characterization of thermally rearranged (TR) polybenzoxazoles: influence of isomeric structure on gas transport properties, Polymer 75 (2015) 199–210.
[44] H. Lin, B.D. Freeman, Materials selection guidelines for membranes that remove CO_2 from gas mixtures, J. Mol. Sci. 739 (2005) 57–74.
[45] H. Lin, B.D. Freeman, Gas permeation and diffusion in cross-linked poly(ethylene glycol diacrylate), Macromolecules 39 (2006) 3568–3580.
[46] G.S. Narang, J.D. Moon, W. Zhang, G.C. Miller, S.R. Choudhury, A. Shaver, B. Vondrasek, J.J. Lesko, J.J. Fallon, M. Bortner, C. D'Ambra, B.D. Freeman, J.S. Riffle, Synthesis and characterization of a phosphine oxide based poly(arylene ether ketone) and blends with poly(2,6-dimethyl-1,4-phenylene oxide) for gas separations, Polymer 138 (2018) 156–168.
[47] J.S. Vrentas, J.L. Duda, Diffusion in polymer—solvent systems. I. Reexamination of the free-volume theory, J. Polym. Sci. Polym. Phys. Ed 15 (1977) 403–416.
[48] M.R. Tant, G.L. Wilkes, An overview of the nonequilibrium behavior of polymer glasses, Polym. Eng. Sci. 21 (1981) 874–895.
[49] L.M. Robeson, The upper bound revisited, J. Membr. Sci. 320 (2008) 390–400.
[50] K. Ghosal, R.T. Chern, B.D. Freeman, W.H. Daly, I.I. Negulescu, Effect of basic substituents on gas sorption and permeation in polysulfone, Macromolecules 29 (1996) 4360–4369.